

Exciton hopping probed by picosecond time-resolved cathodoluminescence

Mehran Shahmohammadi,^{1,a)} Gwénolé Jacopin,¹ Xuewen Fu,² Jean-Daniel Ganière,¹ Dapeng Yu,² and Benoît Deveaud¹

¹Laboratoire d'Optoélectronique Quantique, École Polytechnique Fédérale de Lausanne (EPFL), Station 3, CH-1015 Lausanne, Switzerland

²State Key Laboratory for Mesoscopic Physics, and Electron Microscopy Laboratory, Department of Physics, 209 Chengfu Road, Peking University, Beijing 100871, China

(Received 14 July 2015; accepted 20 September 2015; published online 5 October 2015)

The exciton transport is studied in high quality ZnO microwires using time resolved cathodoluminescence. Owing to the available picosecond temporal and nanometer spatial resolution, a direct estimation of the exciton average speed has been measured. When raising the temperature, a strong decrease of the effective exciton mobility (hopping speed of donor-bound excitons) has been observed in the absence of any remarkable change in the effective lifetime of excitons. Additionally, the exciton hopping speed was observed to be independent of the strain gradient value, revealing the hopping nature of exciton movement. These experimental results are in good agreement with the behavior predicted for impurity-bound excitons in our previously published theoretical model based on Monte-Carlo simulations, suggesting the hopping process as the main transport mechanism of impurity-bound excitons at low temperatures. © 2015 AIP Publishing LLC.

[<http://dx.doi.org/10.1063/1.4932098>]

For a long time, strain engineering has been considered as a powerful strategy to tune the electro-optical properties of semiconductors.^{1,2} Moreover, strain is an unavoidable phenomenon in the properties of semiconductor nanostructures. Strain induced Stark shift of the emission energy in III-Nitride semiconductors,³ the strained silicon application for mobility enhanced transistors,² and the bandgap engineering of nanowires quantum wells with core-shell structure through strain⁴ exemplify some contributions of strain in tuning the electro-optical properties of semiconductors. Semiconductor nanowires are suitable for fundamental studies of strain effects, since one can have access to an extremely large range of compressive and tensile strain by simply deforming the nanowire, without introducing dislocations.^{5,6}

Recently, we have reported on the exciton dynamics in ZnO microwires (MWs) under a uniform strain gradient using picosecond time-resolved (tr) cathodoluminescence (CL) measurements.⁷ Excitons were observed to drift, with the estimated mobility of $1400 \pm 100 \text{ cm}^2/\text{eV/s}$ at 8 K, in the presence of an energy gradient induced by the strain variation across a purely bent ZnO MW at low temperature.

In a complementary study, a Monte-Carlo simulation has been performed to interpret the observed efficient drift of donor-bound exciton ($D^\circ X_A$) under strain gradient at low temperatures.⁸ This model is based on the Miller-Abrahams formalism for the jump rate of excitons in disordered semiconductors.⁹ The hopping rate v_{ij} from one donor i at an energy E_i to another donor j at an energy E_j is given by

$$v_{ij} = \begin{cases} v_0 e^{-2\frac{R_{ij}}{a_0}} & \text{if } E_j < E_i \\ v_0 e^{-2\frac{R_{ij}}{a_0}} e^{-\frac{E_i - E_j}{k_B T}} & \text{if } E_j > E_i, \end{cases} \quad (1)$$

^{a)}Electronic mail: Shahmohammadmehran@gmail.com

where v_0 is the attempt-to-hop frequency, a_0 is the $D^\circ X_A$ Bohr radius, k_B is the Boltzmann constant, R_{ij} is the distance between the two donors, and T is the lattice temperature.

This equation shows that at low enough temperatures, the motion is possible only if the final state is at a lower energy than the initial one. Therefore, the hopping rate is independent of the magnitude of their energy difference: the average speed of excitons should be independent of the value of the energy gradient. However, when raising the temperature, the backward motion of excitons activated by thermal energy affects dramatically the average speed of excitons along the strain gradient. The average speed of $D^\circ X_A$ s predicted to decrease by almost a factor of 10, when raising the temperature from 0 K to 30 K.⁸ Therefore, this model predicts two main features for the hopping process of excitons: (i) the independence of the exciton speed from the energy gradient value at low temperature and (ii) a strong thermal quenching of the exciton speed.

In the present letter, the T-dependence of the $D^\circ X_A$ movement speed under a uniform strain gradient is studied. The high quality of the studied ZnO MWs allows us to investigate the exciton dynamics from $T = 4 \text{ K}$ up to 25 K, while in the studied temperature range $D^\circ X_A$ dominates the carrier recombination with a constant effective lifetime. Moreover, the sample has been designed in order to be subjected to a smaller strain gradient value across the bent region of the ZnO MW. This allows us to study the impact of the strain gradient through comparing our results with previously probed MWs in Ref. 7.

Hexagonal ZnO MWs have been grown by chemical vapor deposition along the c -axis, with diameters ranging between 1 and $3 \mu\text{m}$.⁷ Afterwards, these MWs have been transferred to the surface of a highly doped n-type Si wafer and positioned in the middle of SU8 micropillars, designed for applying the four-point-bending strain to the MWs according to ASTM E855–08 standard. Therefore, the

bending part between the two inner SU8 pillars is expected to be under a pure bending condition.^{7,10}

An Attolight Alalin Chronos 4027 system was used to carry out the tr-CL experiments at an acceleration voltage of 6 kV. The excitation was performed with ~ 1 ps electron pulses at the repetition rate of 80 MHz. The collected CL signal was analyzed by a Jobin-Yvon (iHr320) spectrometer equipped with a Synapse CCD camera and a Hamamatsu streak camera synchronized with the electron pulses. The spatial and temporal resolutions of our tr-CL setup are estimated to be 50 nm and 30 ps, respectively.¹¹ The photoluminescence (PL) measurements were carried out by exciting a single straight ZnO MW using the third harmonic ($\lambda = 280$ nm) of a picosecond mode-locked $\text{Al}_2\text{O}_3:\text{Ti}$ laser (average power of $50 \mu\text{W}$ and repetition rate of 80 MHz).

As indicated by arrows in the low temperature PL spectra of a single unbent ZnO MW in Fig. 1(a), the luminescence is composed of an intense emission of D^0X_A at 3.364 eV, and a weak shoulder of free exciton (FX) at 3.380 eV. Increasing the temperature, the PL intensity of D^0X_A slightly decreases with regard to FXs. Nevertheless,

for temperatures below 40 K, the luminescence is still dominated by D^0X_A emission. Figure 1(b) displays the schematics of the measurement, consisting of a MW bent in a four-point bending configuration and excited by the pulsed electron beam. In the SEM image of the probed MW (Fig. 1(c)), the straight and bent regions of the MW are labeled as I and II, respectively. The accurate circular shape of the bent region of the MW confirms the pure bending deformation in this region. The local strain along the [0001] axis ε_c varies linearly across the MW and is defined by the relative distance from the strain neutral plane and the curvature radius of the strain neutral plane $\varepsilon_c = r/\rho$. The strain gradient across the pure bending cross section of the MW ($\partial\varepsilon_c/\partial r = 1/\rho$) amounts to $0.77\% \mu\text{m}^{-1}$ in the probed ZnO MW. This value is smaller than the value in the previous ZnO MWs ($1.25\% \mu\text{m}^{-1}$) in Ref. 7, owing to the different curvature radii of MWs.

No spectral shift is observed for the straight region at 4 K, when scanning the excitation spot across the MW (Fig. 1(d)). However, the CL spectra in the bent region at 4 K (cf. Fig. 1(e)) consist of a broad emission when the exciting at

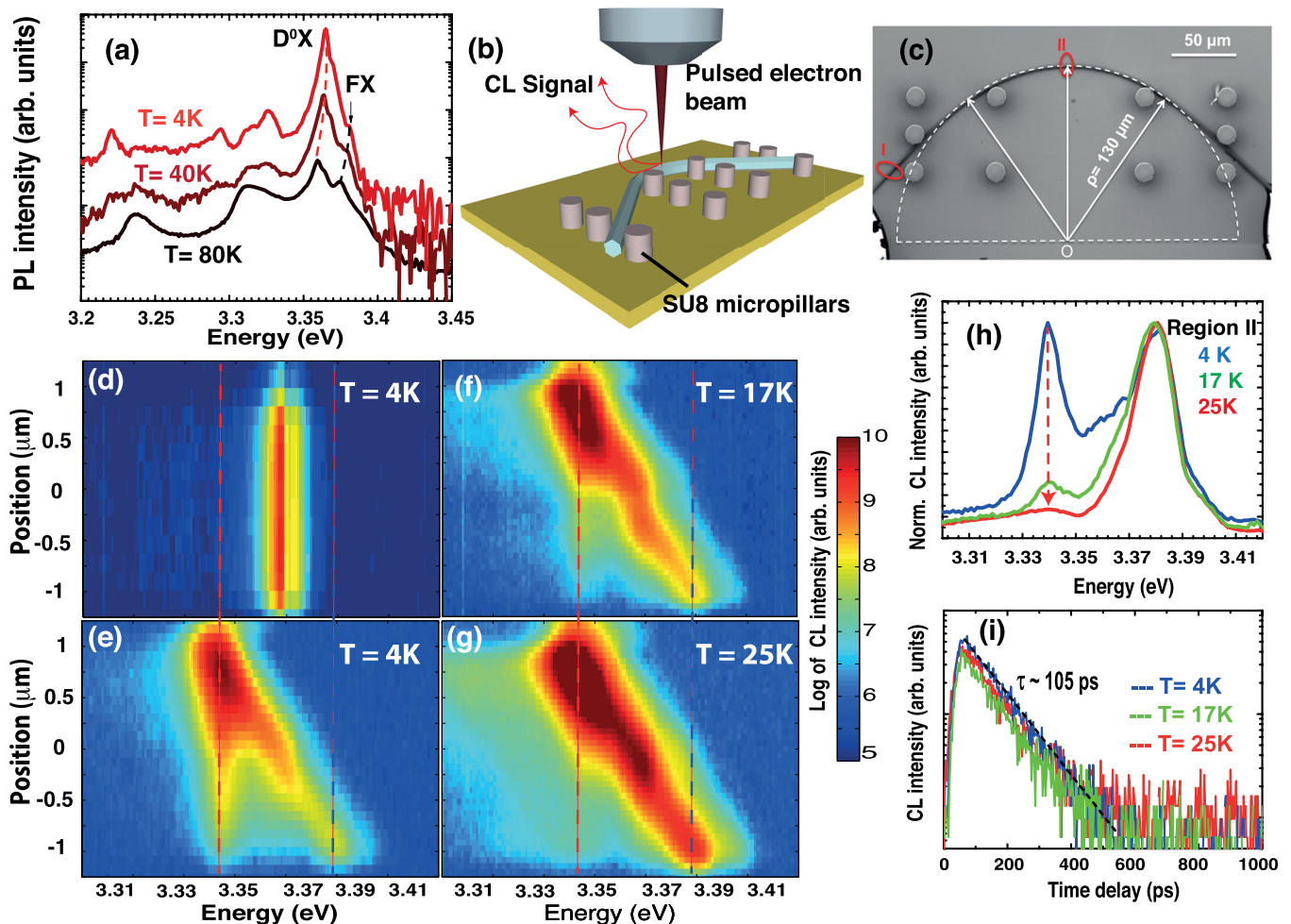


FIG. 1. (a) PL of a single ZnO MW at different temperatures from 4 K to 80 K. The PL spectra are shifted for clarity. (b) Schematics of the tr-CL experiments. (c) SEM image of the probed ZnO MW with a diameter of $d = 2.33 \mu\text{m}$ in a four-point bending configuration. ρ shows the radius of curvature of the neutral plane in the purely bent region. (d) Time-integrated CL spectral mapping of the straight part of MW (part I) as a function of the excitation position across the MW at $T = 4$ K. ((e)–(g)) Time-integrated CL spectra of the bent region of MW (part II) as a function of the excitation position across the MW at $T = 4$ K, 17 K and 25 K, respectively. Strain value changes from $\varepsilon_c = -0.77\%$ in the compressive part (lower part of each panel) to $\varepsilon_c = +0.77\%$ in the tensile part (upper part of each panel). (h) Normalized time-integrated CL spectra in the compressive part (part II) for different temperatures from 4 K to 25 K. The red arrow underlines the decrease in intensity of the low-energy part of the CL spectra. (i) CL decay, integrated over the whole energy of the near-band-edge emission, of the straight part of ZnO MW as a function of temperature.

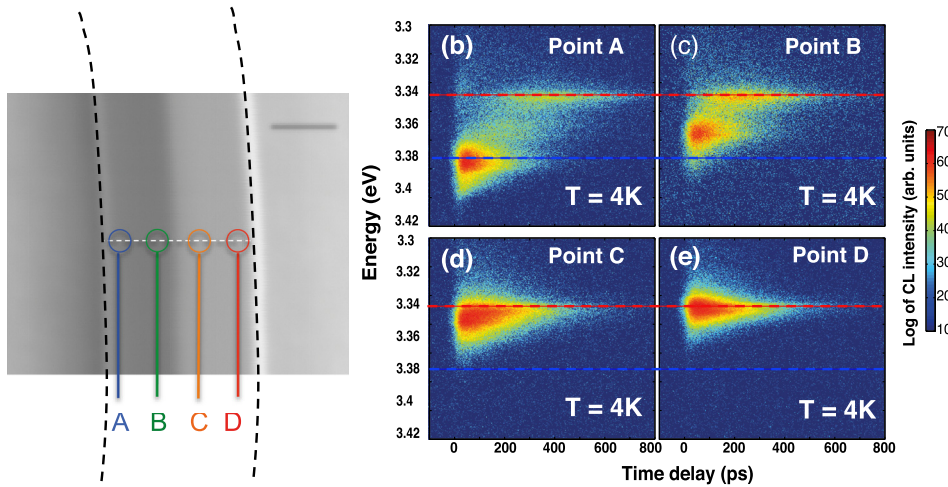


FIG. 2. (a) SEM image of ZnO MW. The position of four equally-spaced excitation spots of A to D is displayed on the SEM image. ((b)–(e)) Streak-camera images obtained by exciting different points (A–D in part (a)) across the bent region of MW at 4 K. Points A–D have an approximate strain value of $\varepsilon_c = -0.57\%$, -0.19% , $+0.19\%$, and $+0.57\%$, respectively.

the interior side of the MW (the lower part of Fig. 1(e)). The CL spectrum progressively redshifts and narrows by moving the excitation spot towards the tensile region (the upper part of Fig. 1(e)). This observation stays consistent with the excitation movement along the energy gradient caused by the strain variation across the MW.⁷ The blue and red dashed lines depict the highest and the lowest emission energies corresponding to the inner and outer edges of the bent region of the ZnO MW, respectively. It is worth noticing that the time-integrated CL spectrum, measured when exciting on the compressive region, consists of two isolated peaks separated by a broad luminescence band: A peak appears on the high-energy side, which shifts when moving the excitation spot, and another one on the lowest energy side, which is independent of excitation position. We attribute the first peak to the fact that, under pulsed excitation conditions, most of the generated excitons recombine close to the excitation spot, i.e., before they can move far distances along the energy gradient. The latter peak, however, originates from the accumulation of excitons on the tensile region of wire (cf. the discussions on the simulations results).

The CL spectra mappings for higher temperatures (cf. Figs. 1(f) and 1(g)) feature a similar redshift of the emission energy, when moving the excitation spot from the compressive part to the tensile part across the bent region of MW. However, the intensity of the low-energy part (around 3.34 eV) appears to decrease strongly when raising the temperature. This decrease of the CL intensity at the tensile part, even more clear on the normalized CL spectra in Fig. 1(h), is due to the decrease in the exciton average speed. The exciton lifetime was measured on the straight part of the MW to be constant (~ 105 ps) over the whole temperature range (cf. Fig. 1(i)). Therefore, we exclude the shortening of the exciton lifetime, when raising the temperature, as the origin of the absence of exciton movement.

The streak images obtained for four equally spaced excitation spots across region II at 4 K are displayed in Fig. 2. The strain value increases linearly from point A (the most compressive region) to point D (the most tensile region). The streak image in Fig. 2(b) features a clear time-dependent redshift of the CL spectrum in addition to a delayed rise at lower energies. These features provide a clear evidence of the exciton movement from regions with higher energies (i.e., with

compressive strain) towards regions with lower energies (i.e., with tensile strain). The streak images corresponding to the middle points across the MW (Figs. 2(c) and 2(d)) also depict the same characteristics as in Fig. 2(b), however, with the CL emission peak starts at lower energies. This clearly evidences the one-directional movement of excitons towards the tensile region. Finally, in the streak image recorded at point D (cf. Fig. 2(e)), no time-dependent redshift in the CL spectrum can be distinguished.

The decay traces, integrated at the highest (blue) and the lowest (red) energy part of the streak images recorded at different temperatures, are displayed in Figs. 3(a)–3(c). In this set of measurements, the excitation spot was always placed in the compressive part of the MW (point A in Fig. 2(a)). The short risetime of CL intensity at compressive region and the delayed risetime for tensile region demonstrate the presence of exciton movement in all these measurements. Despite the absence of any change in the lifetime of excitons in this temperature range, the ratio of the CL intensity in the tensile region compared to the compressive region decreases upon raising the temperature. It is worth noticing that another component with a mono-exponential decay and a much shorter risetime exists in the CL decay of the tensile region. This component features the same decay time as the CL intensity of the compressive part of the MW and a constant intensity ratio to the CL intensity of the compressive region of the MW for all temperatures. According to these characteristics, this component originates from the reabsorption of the luminescence, emitted by the large bandgap regions, by the regions of the MW with lower bandgap.

Since the exciton hopping rate is independent of the energy gradient,⁸ instead of the drift-diffusion model applied in Ref. 7, Equation (2) has been solved by finite difference methods to estimate the exciton speed from our measurements. The term μE representing the exciton drift was replaced by the exciton movement speed v . The carrier density as a function of time and position across the bent MW is then given by

$$\frac{\partial}{\partial t}n(r,t) = -\frac{1}{\tau}n(r,t) + D\frac{\partial^2 n(r,t)}{\partial r^2} - v\frac{\partial n(r,t)}{\partial t}, \quad (2)$$

where n , τ , and D denote the carrier density, the exciton effective lifetime, and the diffusion coefficient, respectively.

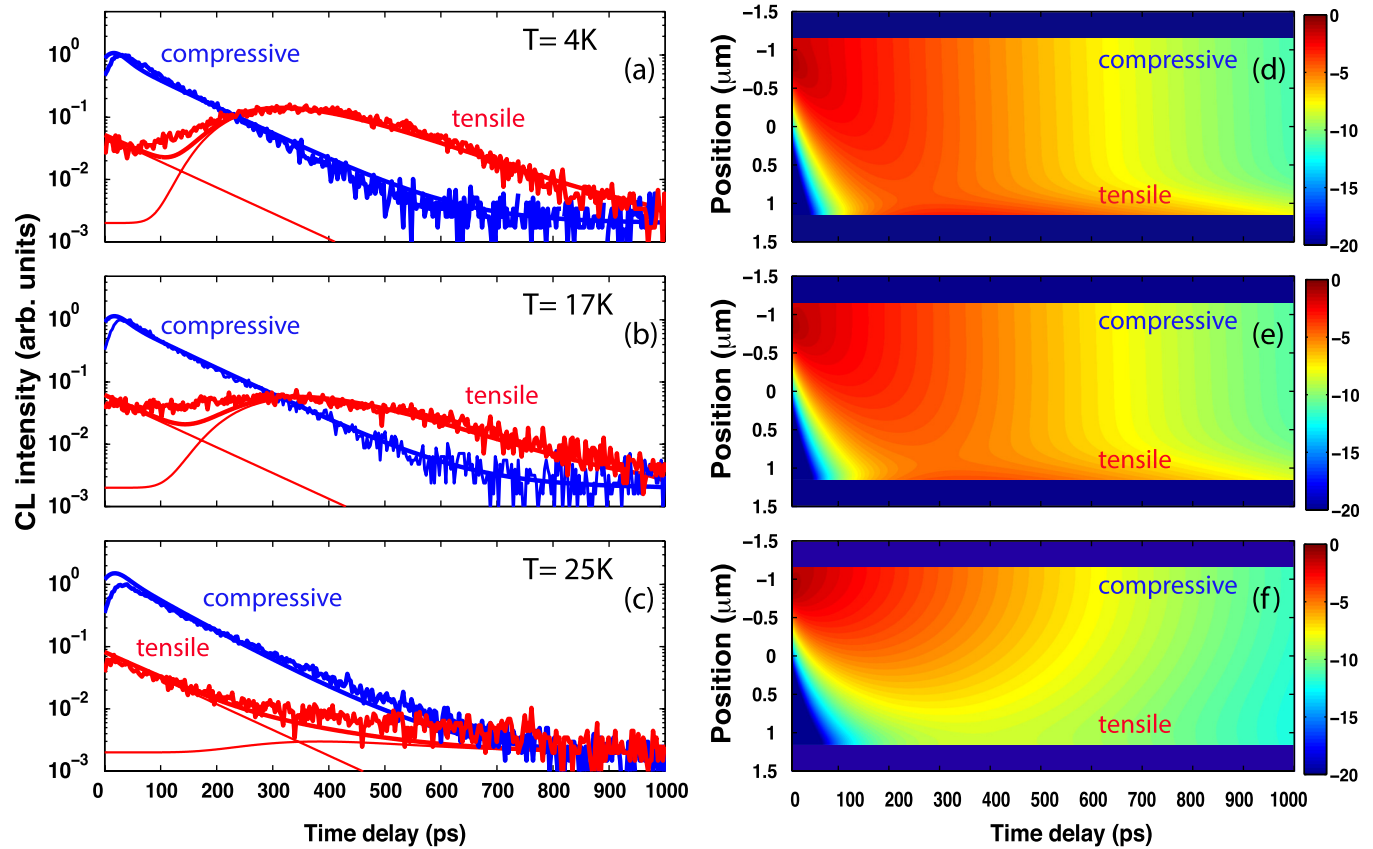


FIG. 3. ((a)–(c)) The CL intensity decay at the highest (blue) and lowest (red) emission energy extracted from streak images recorded at 4 K, 17 K, and 25 K, respectively. The results of drift-diffusion simulation are shown for comparison with experimental data. ((d)–(f)) Simulation results for the CL intensity across the bent region of MW as a function of time delay after the excitation for 4 K, 17 K, and 25 K, respectively. In all the experiments and simulations, the excitation spot is placed in the most compressive region across the MW (point A in Fig. 2(a)).

The boundary conditions have been implemented by adding another term due to the non-radiative recombination at the edge of the MW ($|r| = d/2$)¹²

$$\frac{\partial}{\partial t} n(d/2, t) = -\frac{1}{\tau} n(d/2, t) + D \frac{\partial^2 n(d/2, t)}{\partial r^2} - v \frac{\partial n(d/2, t)}{\partial t} - \frac{1}{\tau_{surf.}} n(d/2, t), \quad (3)$$

where $\tau_{surf.}$ denotes the exciton lifetime at surface of the MW. The surface recombination velocity $v_{surf.}$, independent of discretization procedure, can be defined according to

$$v_{surf.} = \frac{\Delta r}{\tau_{surf.}}, \quad (4)$$

where Δr is the size of the discretization step.

The effective lifetime of excitons is taken to be 105 ps and constant for all temperatures, a value measured on the straight part of the MW. The exciton movement speed v and the diffusion constant D were tuned as the main fitting parameters to reproduce well the decay time and risetime time of CL decays at the compressive and tensile part of the MW, as well as their relative intensity. The intense CL in the tensile region of the MW indicates the accumulation of the excitons at the edge of the MW in the absence of a fast non-radiative channel, which is consistent with the smaller value of the $v_{surf.} = 5 \times 10^3$ cm/s compared to the previously

probed MWs in Ref. 7. A mono-exponential decay function with a constant proportion to the CL intensity at compressive part is added to the simulation results to mimic the component from reabsorption of light in the tensile region of MW. The results of the simulations have been convoluted with a Gaussian function with temporal broadening of 30 ps to account for the temporal resolution of our experimental system.

The exciton movement speed from these simulations was estimated to $v = 5.8 \pm 0.2$ nm/ps at 4 K, $v = 4.2 \pm 0.2$ nm/ps at 17 K, and $v = 0.4 \pm 0.2$ nm/ps at 25 K. The diffusion coefficient was considered to be constant over this temperature range and estimated to $D = 7 \pm 3$ cm²/s. The results of these finite element simulations are shown to be in good agreement with the experimental results (cf. Figs. 3(a)–3(c)).

To ensure the reliability of the estimated exciton speed, one can compare the risetime of the CL intensity for the compressive and tensile part of MW: It takes about 350 ps for an exciton to travel from the high-energy to the low-energy side of the MW (see Fig. 3(a)). Thus, the average speed of excitons for traveling this distance ($d \approx 2 \mu\text{m}$) is determined to be 5.7 nm/ps at 4 K, which is in a close agreement to our simulation results. Although the simulation results do not vary significantly with the diffusion constant, our estimated value for D stays in reasonable agreement with the previous reports in the literature Ref. 13. Note further that according to the Einstein-Smoluchowski relation,¹⁴ the ratio of the diffusion constant to the mobility should be

linearly dependent on the temperature in a non-degenerate semiconductor under quasi-equilibrium condition. However, since the movement of $D^{\circ}X_A$ excitons is governed by a hopping process and not by a Brownian motion as is the case for FXs, the universality of the Einstein relation can be violated for exciton hopping in disordered materials.^{15–17} Such an investigation, however, lies beyond the scope of the present letter.

Comparing the results obtained here with our previous results reported in Ref. 7, some remarkable differences should be noticed. First, despite the difference in the strain gradient value in the probed MWs, the estimated value for exciton movements speed at $T \leq 10$ K remains approximately the same in both studies. As mentioned before, in the absence of thermal energy, excitons can hop from one energy state to the next one as long as the next donor is placed at a lower energy. Therefore, this process is independent of the energy difference between two donor states at low temperature.

Then, the determinant parameters in the hopping speed are the a_0 and the R_{ij} , i.e., the doping concentration. Since ZnO MWs in both studies have been grown under the same conditions, neither the type of dopant nor the doping concentration are expected to vary between these two samples. The latter confirms the main outcome from our theoretical proposal that, at low temperatures, the value of the energy gradient is not determining the hopping speed of impurity-bound excitons. Therefore, at low temperature, in such system, it is better to describe the motion of exciton in terms of an average speed rather than of a mobility. Our experimental results show also that the average speed of $D^{\circ}X_A$ s along the strain gradient has a strong T-dependence. The 10-fold decrease of the exciton movement speed from 4 K to 25 K originates from the thermally activated backward motion of excitons. This strong T-dependence of exciton average speed evidences the exciton hopping as the main process of exciton movement at low temperatures.

In conclusion, we presented a direct study of exciton movement under a uniform strain gradient in ZnO MWs at low temperatures. The same movement speed for impurity-bound excitons has been observed in the presence of different energy gradient values across the probed MWs. These results show the minor role played by the strain gradient value in the exciton hopping at low temperatures, and confirm the critical role of the doping concentration. The observed dramatic T-dependence of the exciton speed proves the validity of the hopping mechanism as the main transport mechanism of impurity-bound excitons at low temperatures. These results are expected to be general and may be applied to other materials.

The present work was financially supported by the Swiss National Science Foundation under Project Nos. 153620 and 154853, the EPFL fellowship program co-funded by Marie Curie (FP7 Grant Agreement No. 291771), the National Science Foundation of China (NSFC 11234001), and by the National 973 Program of China (2013CB932602).

- ¹R. He and P. Yang, "Giant piezoresistance effect in silicon nanowires," *Nat. Nanotechnol.* **1**, 42 (2006).
- ²M. Jeong, B. Doris, J. Kedzierski, K. Rim, and M. Yang, "Silicon device scaling to the sub-10-nm regime," *Science (New York)* **306**, 2057 (2004).
- ³M. Leroux, N. Grandjean, M. Laugt, J. Massies, B. Gil, P. Lefebvre, and P. Bigenwald, "Quantum confined Stark effect due to built-in internal polarization fields in (Al,Ga)N/GaN quantum wells," *Phys. Rev. B* **58**, R13371 (1998).
- ⁴G. Jacopin, L. Rigutti, S. Bellei, P. Lavenus, F. H. Julien, A. V. Davydov, D. Tsvetkov, K. A. Bertness, N. A. Sanford, J. B. Schlager, and M. Tchernycheva, "Photoluminescence polarization in strained GaN/AlGaIn core/shell nanowires," *Nanotechnology* **23**, 325701 (2012).
- ⁵T. Zhu and J. Li, "Ultra-strength materials," *Prog. Mater. Sci.* **55**, 710–757 (2010).
- ⁶C. P. Dietrich, M. Lange, F. J. Klüpfel, H. Von Wenckstern, R. Schmidt-Grund, and M. Grundmann, "Strain distribution in bent ZnO microwires," *Appl. Phys. Lett.* **98**, 031105 (2011).
- ⁷X. Fu, G. Jacopin, M. Shahmohammadi, R. Liu, M. Benameur, J.-D. Ganière, J. Feng, W. Guo, Z. M. Liao, B. Deveaud, and D. Yu, "Exciton drift in semiconductors under uniform strain gradients: Application to bent ZnO microwires," *ACS Nano* **8**, 3412 (2014).
- ⁸G. Jacopin, M. Shahmohammadi, J.-D. Ganière, and B. Deveaud, "Hopping process of bound excitons under an energy gradient," *Appl. Phys. Lett.* **104**, 042109 (2014).
- ⁹A. Miller and E. Abrahams, "Impurity conduction at low concentrations," *Phys. Rev.* **120**, 745 (1960).
- ¹⁰X. W. Fu, Z. M. Liao, R. Liu, J. Xu, and D. Yu, "Size-dependent correlations between strain and phonon frequency in individual ZnO nanowires," *ACS Nano* **7**, 8891 (2013).
- ¹¹M. Merano, S. Sonderegger, A. Crottini, S. Collin, P. Renucci, E. Pelucchi, A. Malko, M. H. Baier, E. Kapon, B. Deveaud, and J.-D. Ganière, "Probing carrier dynamics in nanostructures by picosecond cathodoluminescence," *Nature* **438**, 479 (2005).
- ¹²B. Lambert, F. Clerot, B. Deveaud, A. Chomette, G. Talalaeff, A. Regreny, and B. Sermage, "Electron and hole transport properties in GaAs-AlGaAs superlattices," *J. Lumin.* **44**, 277 (1989).
- ¹³J. Yoo, B. Chon, W. Tang, T. Joo, L. S. Dang, and G. C. Yi, "Excitonic origin of enhanced luminescence quantum efficiency in MgZnO/ZnO coaxial nanowire heterostructures," *Appl. Phys. Lett.* **100**, 223103 (2012).
- ¹⁴A. Einstein, "Über die von der molekularkinetischen Theorie der Wärme geforderte Bewegung von in ruhenden Flüssigkeiten suspendierten Teilchen," *Ann. Phys.* **322**, 549 (1905).
- ¹⁵L. Li, N. Lu, M. Liu, and H. Bässler, "General Einstein relation model in disordered organic semiconductors under quasiequilibrium," *Phys. Rev. B* **90**, 214107 (2014).
- ¹⁶G. A. Wetzelaer, L. J. A. Koster, and P. W. M. Blom, "Validity of the Einstein relation in disordered organic semiconductors," *Phys. Rev. Lett.* **107**, 066605 (2011).
- ¹⁷K. Harada, A. G. Werner, M. Pfeiffer, C. J. Bloom, C. M. Elliott, and K. Leo, "Organic homojunction diodes with a high built-in potential: Interpretation of the current-voltage characteristics by a generalized Einstein relation," *Phys. Rev. Lett.* **94**, 036601 (2005).